Am J Cancer Res 2021;11(6):3039-3054
www.ajcr.us /ISSN:2156-6976/ajcr0126779

Original Article

Honokiol induces ferroptosis in colon cancer cells by regulating GPX4 activity

Cao Guo[1,2,3], Ping Liu[1,3], Ganlu Deng[4], Ying Han[1,3], Yihong Chen[1,3], Changjing Cai[1,3], Hong Shen[1,2,3], Gongping Deng[5], Shan Zeng[1,3]

[1]Department of Oncology, Xiangya Hospital, Central South University, Changsha 410008, Hunan, China; [2]Key Laboratory for Molecular Radiation Oncology of Hunan Province, Xiangya Hospital, Central South University, Changsha 410008, Hunan, China; [3]National Clinical Research Center for Geriatric Disorders, Xiangya Hospital, Central South University, Changsha 410008, Hunan, China; [4]Department of Oncology, The First Affiliated Hospital of Guangxi Medical University, Shuangyong Road, Nanning 530021, Guangxi Zhuang Autonomous Region, China; [5]Department of Emergency, Hainan General Hospital, Hainan Affiliated Hospital of Hainan Medical University, 19 Xiuhua Road, Haikou 570311, Hainan, China

Received November 22, 2020; Accepted May 14, 2021; Epub June 15, 2021; Published June 30, 2021

Abstract: Colon cancer (CC) is a prevalent malignancy worldwide. Approaches to specifically induce tumor cell death have historically been a popular research topic. Honokiol (HNK), which exhibits highly efficient and specific anticancer effects, is a biphenolic compound found in *Magnolia grandiflora*. In the present study, we aim to study the effect of HNK on CC cells and elucidate the potential underlying mechanisms. Seven CC cell lines (RKO, HCT116, SW48, HT29, LS174T, HCT8, and SW480) were used. Cells were exposed to HNK and subjected to a series of assays to evaluate characteristics such as cellular activity, reactive oxygen species (ROS) levels and ferroptosis-related protein expression levels. Lentiviral transduction was also used to verify molecular mechanisms in vivo and in vitro. We here observed that HNK reduced the viability of CC cell lines by increasing ROS and Fe^{2+} levels. Transmission electron microscopy revealed HNK-induced changes in mitochondrial morphology. HNK decreased the activity of Glutathione Peroxidase 4 (GPX4) but did not affect system Xc-. Thus, our datas indicated that HNK can induce ferroptosis in CC cells by reducing the activity of GPX4. As a potential therapeutic drug, HNK showed good anticancer effects through diverse signal transduction mechanisms and multiple pathways.

Keywords: Honokiol (HNK), ferroptosis, reactive oxygen species (ROS), colon cancer (CC), GPX4

Introduction

Over the past decade, researchers have investigated various methods to induce programmed cell death. Apoptosis is the primary form of programmed cell death induced by different anticancer drugs [1, 2]. However, nonapoptotic forms of cell death, such as autophagy and regulatory necrosis, have recently attracted considerable interest [3]. As cancer cells resist apoptosis almost systematically, these nonapoptotic forms are increasingly considered to be a prospective area of research to improve cancer treatment [4, 5].

Recently, "ferroptosis", a newly identified type of cell necrosis, has gradually gained attention [6, 7]. Unlike events during other forms of cell death, such as cell membrane rupture and content release during necrosis, double-layer autophagic vacuole formation during autophagy or chromatin condensation during apoptosis [8], the causative event of ferroptosis is the failure of glutathione (GSH)-dependent antioxidant defense systems. Ferroptosis does not lead to morphological changes but is distinguished by a number of lipid reactive oxygen species (ROS) and a decrease in the density of the mitochondrial membrane [9-11].

According to previous reports of ferroptosis, iron ions are not only important trace elements in the human body but are also the primary particles involved in the occurrence of ferroptosis [12]. The main form of extracellular circulating iron is the trivalent iron cation (Fe^{3+}). Fe^{3+} enters the cell membrane through the iron transfer protein Transferrin (TFR) and is then localized in

the nucleosome, where it is reduced to ferrous iron (Fe^{2+}) through the iron reductase activity of Six-Transmembrane Epithelial Antigen of Prostate 3 (STEAP3). Finally, divalent metals mediate the release of Fe^{2+} from the nucleus into the unstable iron pool in the cytoplasm mediated by membrane iron transporters (e.g., Ferroportin, FPN1) [13]. The imbalance between Transferrin and Ferroportin can increase the intracellular content of Fe^{2+}. Excessive iron results in ROS production through the Fenton reaction and eventually induces ferroptosis.

Ferroptosis inducers and inhibitors have recently been reported. For example, classic inducer erastin reduces GSH levels by directly inhibiting the activity of the cystine/glutamate antiporter system Xc- [14, 15]. This process accelerates the accumulation of ROS during ferroptosis. Other ferroptosis inducers and inhibitors include RSL3, RSL5, and the first-line chemotherapeutic drug for hepatocellular carcinoma, sulfasalazine [16, 17]. Most antitumor drugs reported to date exert their anticancer effects through a variety of molecular regulatory mechanisms. For example, Guang Liang et al. found that in head and neck carcinoma, Dihydroartemisinin induced ferroptosis and caused cell cycle arrest [18]. Understanding the mechanisms underlying the anticancer effects of these effective natural pharmaceutical ingredients is highly valuable for fully exploring the potential of drugs and for developing new ideas for tumor therapy.

Honokiol (HNK) is a bisphenol compound that can be extracted from various parts of *Magnolia officinalis* [19]. HNK has been reported to inhibit the growth of various cancers in vitro and in vivo by inducing apoptosis and cell cycle arrest and is thus considered a highly versatile cancer cell "killer" because it can induce cell death through both nonapoptotic and apoptotic mechanisms [20-22]. However, the mechanisms underlying the antitumorigenic activities of HNK are undefined.

In this study, we utilized a panel of CC lines to investigate the biological antitumor effects of HNK.

Materials and methods

Chemicals and antibodies

The small molecule drug HNK was obtained from Selleck Chemicals (Houston, TX, USA). The iron ion chelating agent deferoxamine (DFO), was also purchased from Selleck Chemicals. The rabbit primary antibody specific for GPX4 was purchased from Cell Signaling Technology (CST, Danvers, MA). Primary antibodies specific for Transferrin and Ferroportin were purchased from Abcam (Cambridge, MA, UK). The primary antibody specific for GAPDH, which was used as the loading control, was purchased from Proteintech (Wuhan, China).

Cell culture

The human CC cell lines SW48, HT29, LS174T, HCT116, HCT8, RKO, and SW480 were obtained from the Xiangya Medical College Cell Bank Institutes (Changsha, China). The cells were cultured in 25-cm^2 flasks in RPMI-1640 medium or DMEM supplemented with 10% fetal bovine serum, penicillin, and streptomycin. These cells were cultured in flasks at 37°C in a 5% CO_2 incubator.

ROS determination

The level of intracellular ROS was determined with a 2,7-Dichlorodi-hydrofluorescein diacetate (DCFH-DA) probe (Solarbio, Beijing, China). Cells were seeded in a 6-well plate and incubated with HNK for 12 h. The original DCFH-DA solution was diluted 1:1000 with serum-free medium and was then added to each well and incubated at 37°C for 20 min. Cells were collected and washed three times with PBS solution to remove the residual DCFH-DA probe. The fluorescence intensities of the resuspended cells were measured in a flow cytometer using a 488 nm excitation wavelength and a 525 nm bandpass filter for DCF detection (FACSCanto II, BD Biosciences, San Jose, CA).

Cell death assay

Cell death was assessed using a Cell Counting Kit-8 (CCK8, Biosharp, Hefei, China). In brief, 2×10^5 cells were inoculated in a 96-well cell culture plate. After 12 h, HNK was added to the complete culture medium at the following final concentrations: 0, 0.1, 1, 10, 20, 30, 50, 70, and 100 μM. Then, 10 μL of CCK8 reagent was added to each well and incubated at 37°C for 1 h. The OD value of each well was measured at 450 nm, and the cell survival rate was calculated. Quantification was performed from data generated in at least 3 independent experiments.

We also used an Annexin V/PI apoptosis detection kit (BD Biosciences) to determine the cell death rate. In brief, after the indicated treatments, cells were collected and resuspended in 500 μL of binding buffer. FITC-conjugated Annexin V reagent (5 μL) was added, and cells were stained for 10 min. Then, 1 μL of PI was added and incubated for 5 min. The cell death rate was determined with a FACSCalibur flow cytometer (BD Biosciences) and FlowJo software. These assays were performed in triplicate.

Fe^{2+} level measurement

The level of Fe^{2+} was measured using Mito-FerroGreen (Dojindo Molecular Technologies, Tokyo, Japan). In brief, cells were seeded on TC-treated crawlers and subjected to different treatments. Then, the Mito-FerroGreen working solution (5 μM, 200 μL) was added to the cells and incubated for 30 min. The supernatant was discarded, and the cells were washed three times with HBSS. A serum-free medium containing HNK and/or DFO was added to the cells and incubated for 6 h in a 5% CO_2 atmosphere. The cells were observed by confocal fluorescence microscopy.

Transmission electron microscopy

The mitochondrial morphology of cells was inspected using a transmission electron microscope made by Biofcen Corporation (Shanghai, China). Treated cells were washed with PBS, and cell clusters were collected by centrifugation. Cell clusters were fixed with glutaraldehyde (2.5%) solution overnight at 4°C. The samples were sent to the Biofcen Company after osmium tetroxide treatment, acetone dehydration, Duruban resin embedding, and lead citrate staining. Sections (70 nm) were imaged with a JEM1230 electron microscope (JEOL Corporation, Tokyo, Japan) at 40-120 kV.

Western blot analysis

Total protein was extracted from cells with RIPA lysis buffer, and the protein concentration was determined with a BCA kit (Biosharp). Proteins (40 μg) were separated by 10% SDS-PAGE and subsequently transferred to PVDF membranes (0.45 μm). After blocking for 1 h, these membranes were incubated overnight at 4°C with primary antibodies (anti-Transferrin, anti-Ferroportin, anti-GPX4, and anti-GAPDH). The next day, the membranes were washed in TBST solution and incubated with the secondary antibodies for 1 h at room temperature. Bands were visualized in a ChemiDoc XRS+ system (Bio-Rad, Hercules, CA). GAPDH was used as the endogenous reference.

Construction of cell lines with GPX4 overexpression

To explore the role of GPX4 in vivo and in vitro, the candidate human GPX4 sequence containing the open reading frame (GenBank Accession No: NM_002085) was cloned into the plenti-EF1a-P2A-Puro-CMV-MCS-3Flag vector to generate GPX4 overexpression plasmid, and a lentiviral vector was constructed by Obio Technology (Shanghai) Corp., Ltd. We defined cells transfected with GPX4 or vector plasmids as GPX4-overexpression (GPX4-OE) or vector. And cells infected by lentivirus were named as lentivirus-GPX4 (Lv-GPX4) or lentivirus-negative control (Lv-NC).

The titers of Lv-GPX4 and the vector-containing lentivirus were 1×10^7 TU/mL. The constructed plasmids and lentivirus were transfected into cells using Lipofectamine 3000 reagent. Puromycin was used to screen stable CC cell lines with overexpression of GPX4. Constructed plasmids were used for in vitro experiments and lentivirus for animal experiments. Transfection efficiency was confirmed by qRT-PCR and western blot.

Glutamic acid and GSH measurement

A glutamic acid detection kit was purchased from Sigma (catalog number MAK004, St. Louis, MO). In brief, the reaction mixes were set up based on the scheme in the protocol supplied by Sigma, and standard curves were generated. A total of 1×10^6 cells were collected in assay buffer (150 μL) and subsequently homogenized. The cells were centrifuged at 13000×g for 10 min to remove insoluble material. Each well was mixed by vortexing and incubated at 37°C for 30 min. The intracellular glutamate content was measured according to the absorbance of the marker enzyme at 450 nm.

A Total Glutathione Assay Kit was purchased from Beyotime Corporation (catalog number S0052, Beyotime Biotechnology, China). Cells

were collected for removal of the supernatant after centrifugation. An appropriate amount of reagent S was added, and the samples were fully vortexed to remove protein. Then, the samples were subjected to two rapid freeze-thaw cycles using liquid nitrogen and a 37°C water bath, placed at 4°C or in an ice bath for 5 min, and centrifuged at 10000×g for 10 min at 4°C. The supernatant was collected for determination of the total GSH content. The sample or standard product was added sequentially to a 96-well plate, and the absorbance of the marker enzyme at 405 nm was measured to generate the standard curve and calculate the total GSH content.

Xenograft models

Ten BALB/c nude mice (male, 4 weeks old, 18.0 ± 2.0 g) were randomly divided into two groups for the in vivo xenograft assay. Mice were injected with 5×10^6 RKO cells with stable overexpression GPX4 (described Lv-GPX4 group), control vector (described Lv-NC group). Cells were subcutaneously injected into the right anterior axilla of mice in both groups. Mice then received HNK (0.5 mg/kg/w) by intraperitoneal injection for 4 weeks. The subcutaneous tumor volumes in the nude mice in the two groups were recorded every two days. All animal experiments and procedures were directed and approved by the Experimental Animal Ethics Committee of Central South University (20170232).

Statistical analysis

The data are presented as the mean ± SD values and were analyzed with GraphPad Prism software (Version 7.04, San Diego, CA). Student's t-test and one-way ANOVA followed by post hoc tests for multiple comparisons were used to compare the differences between 2 groups and more than 2 groups of data, respectively. A difference was considered to be statistically significant only if the *P*-value was less than 0.05.

Results

HNK reduced the viability of CC cells

CCK8 assays were conducted to assess viability after cells were exposed or not exposed to HNK for 24 h and 48 h. The abovementioned 7 cell lines represented different subtypes of CC. All seven cell lines showed dose-dependent and time-independent reductions in viability in response to HNK ($P<0.05$, **Figure 1A-C**). Since only a few cells were alive 48 h after HNK incubation, we selected 24 h as the time point for further in these experiments. The concentration of HNK that decreased cell viability by 50% (IC_{50}) ranged from 11.42 μM for RKO cells to 47.65 μM for HCT116 cells. According to the IC_{50} value, we selected two of the cell lines with the highest sensitivity to HNK-i.e., RKO (11.42 μM) and SW480 (15.14 μM). Previous studies showed that the molecular mechanism of HNK acts through a reduction in tumor cell viability via the apoptotic pathway. Our results showed that HNK induced CC cell death in a dose-dependent manner.

HNK increased the levels of ROS and Fe^{2+} in CC cells

ROS are byproducts generated from the normal mitochondrial respiration. A variety of antitumor drugs kill tumor cells by increasing ROS. Here, we investigated the specific molecular mechanism by which HNK kills CC cells. We investigated the ROS levels in SW480 and RKO cells after incubation with HNK at different concentrations for 24 h.

Recently, ferroptosis has been favored by researchers as a newly identified type of unprogrammed cell death. Ferroptosis is characterized by the accumulation of lipid peroxide and Fe^{2+} ion. Therefore, we first measured the level of ROS and Fe^{2+} ion. As displayed in **Figure 2A**, HNK increased the ROS level in a dose-dependent manner in CC cells ($P<0.05$). We then introduced deferoxamine (DFO), an iron ion chelating agent which can significantly inhibit the occurrence of ferroptosis, and divided the cells into four groups: the NC group, HNK group, DFO group, and HNK+DFO group. The survival rate of the cells in each group was measured by CCK8 assay. As shown in **Figure 2B** and **2C**, DFO significantly impaired HNK-induced CC cell death ($P<0.05$, **Figure 2B** and **2C**). The Fe^{2+} ion level was determined by Mito-FerroGreen fluorescent dye. The green fluorescence in the cytoplasm in **Figure 2D** presented the staining by Mito-FerroGreen a specific probe for labeling of Fe^{2+} ions. The green fluorescence signal in HNK group cells was significantly enhanced as compared with that in NC group cells ($P<0.05$, **Figure 2D**). However, the fluorescence signal in DFO group cells was significantly reduced compared with that in NC group cells ($P<0.05$).

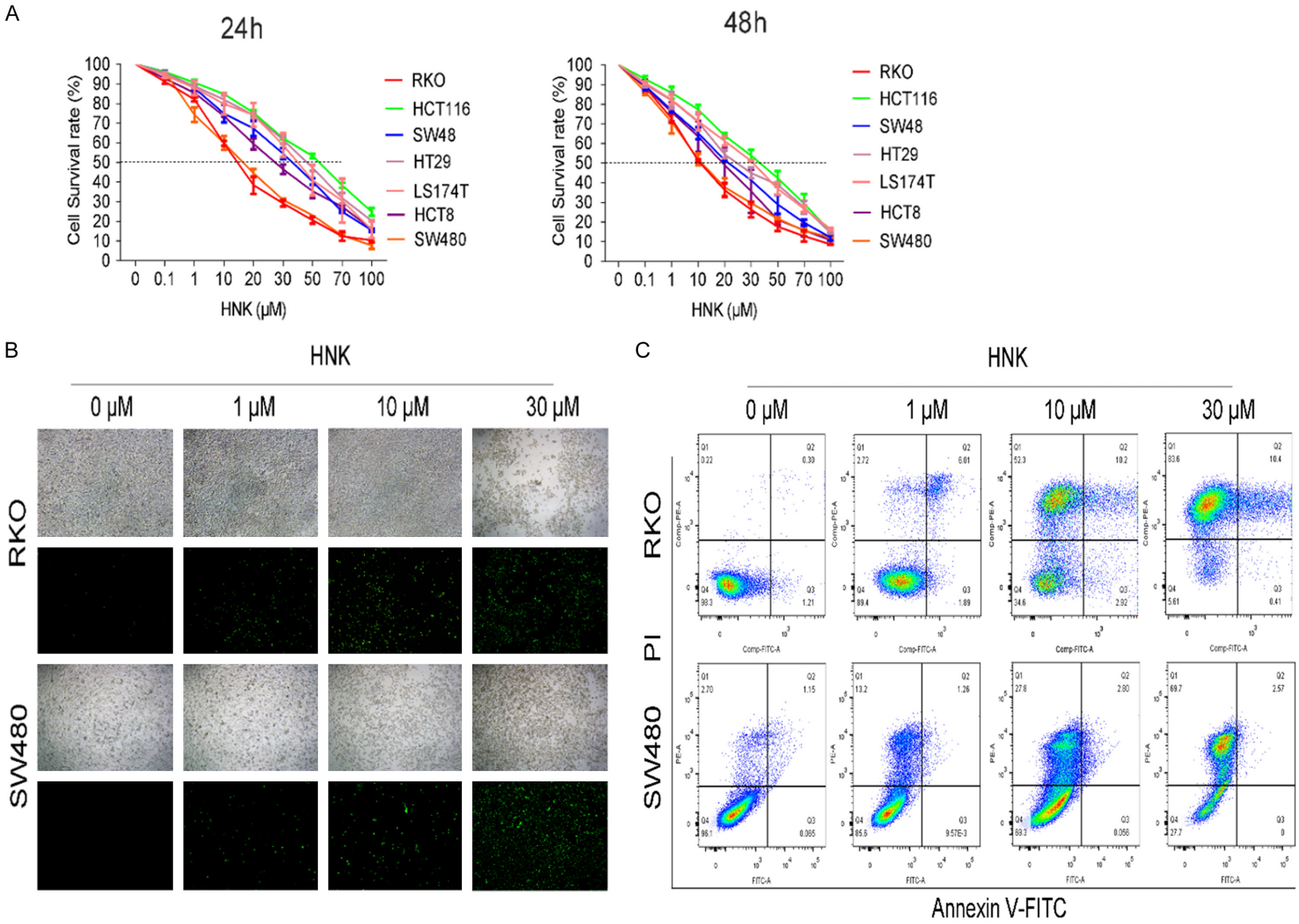
A
24h
48h
Cell Survival rate (%)
HNK (μM)
RKO
HCT116
SW48
HT29
LS174T
HCT8
SW480
B
HNK
0 μM
1 μM
10 μM
30 μM
RKO
SW480
C
HNK
0 μM
1 μM
10 μM
30 μM
RKO
SW480
PI
Annexin V-FITC

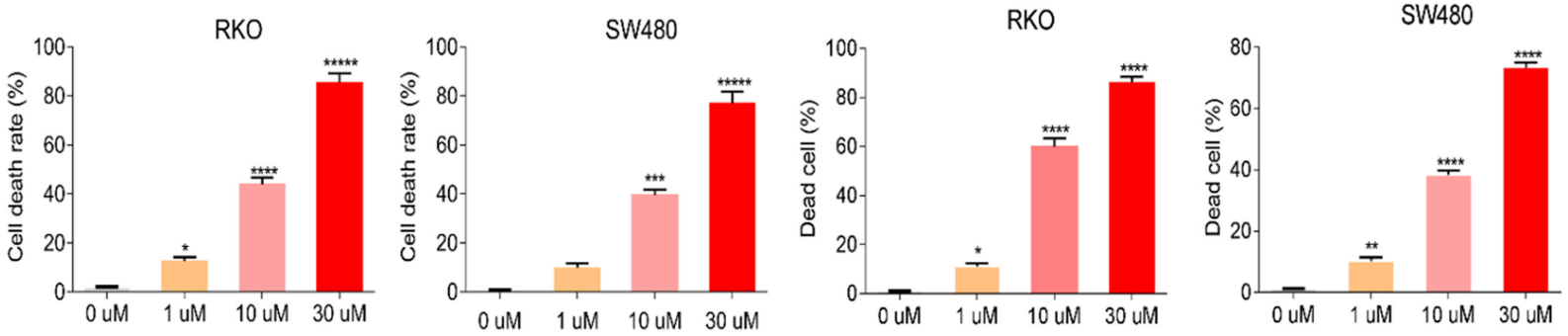

Figure 1. HNK reduced the viability of CC cells. A. To evaluated the anti-tumor effect of HNK on CC cells, A CCK8 assay was carried out to determine the IC_{50} values of HNK in six CC cell lines at 24 h and 48 h. B. Sytox staining was also used to assess cell death in CC cells treated with different concentrations of HNK (original magnification: 100×). The green fluorescent labeled cells are dead cells in the image, while others without fluorescent labeled are live cells. C. The cell death rates of RKO and SW480 cells were determined by flow cytometry with Annexin V/PI staining. And cells were incubated or not incubated with HNK for 48 h. The data are shown as the mean ± SD values. Compared to 0 μM group, *: P<0.05, **: P<0.01, ***: P<0.001, ****: P<0.0001.

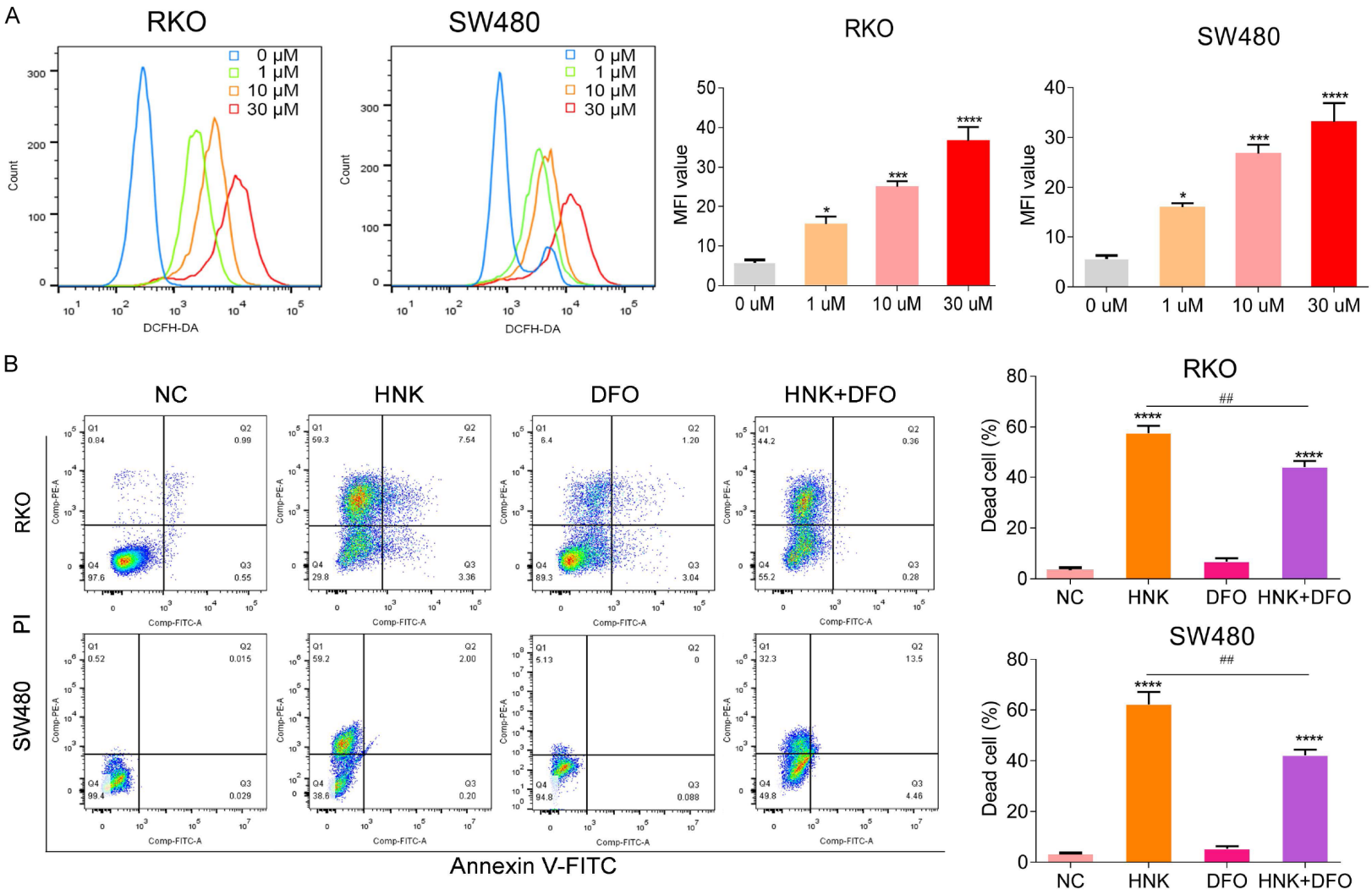
A
RKO
SW480
0 μM
1 μM
10 μM
30 μM
Count
DCFH-DA
MFI value
0 uM
1 uM
10 uM
30 uM
B
NC
HNK
DFO
HNK+DFO
RKO
PI
SW480
Annexin V-FITC
Comp-PE-A
Comp-FITC-A
Dead cell (%)
##

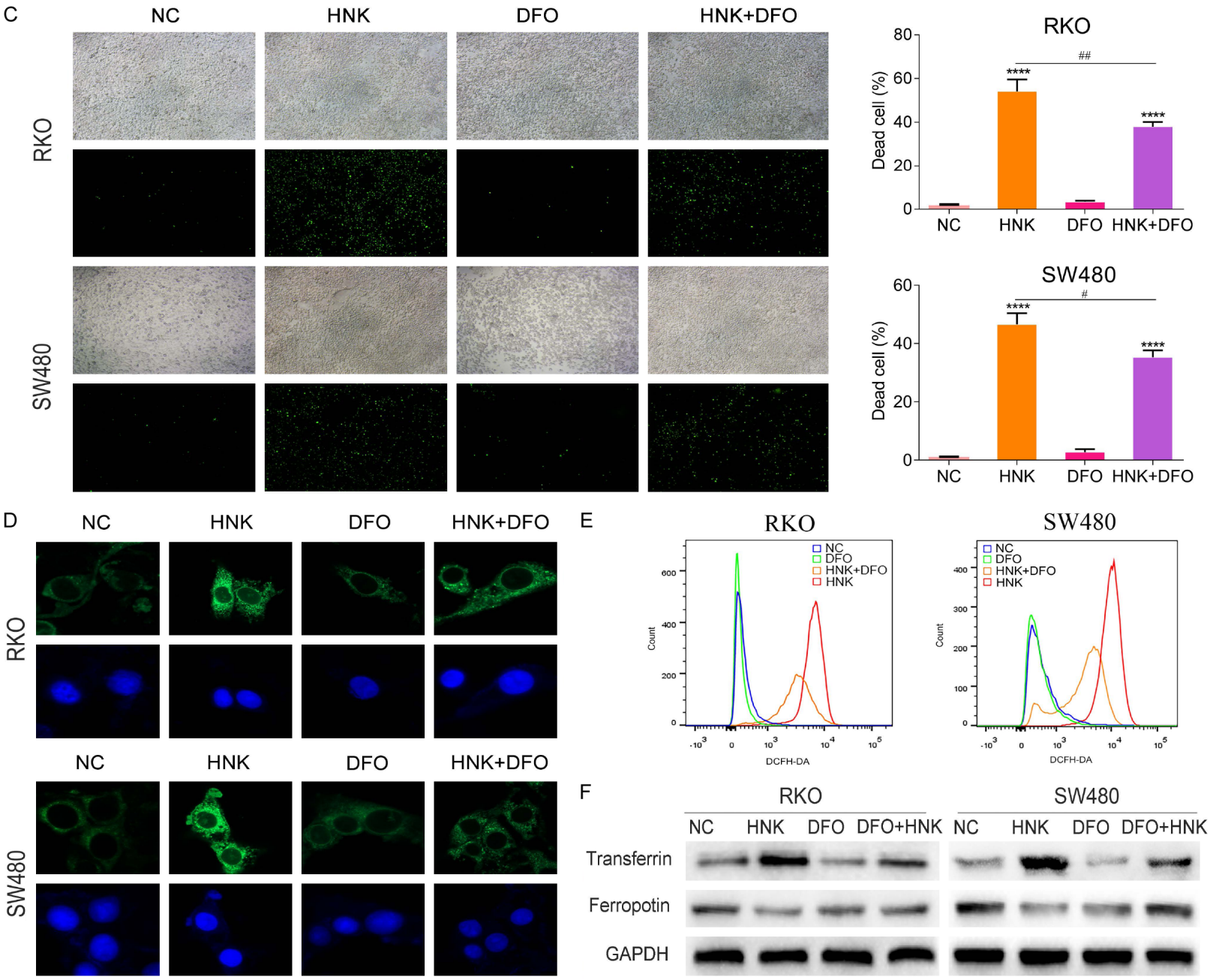
C
NC
HNK
DFO
HNK+DFO
RKO
SW480
RKO
Dead cell (%)
80
60
40
20
0
##
****
****
NC
HNK
DFO
HNK+DFO
SW480
Dead cell (%)
60
40
20
0
#
****
****
NC
HNK
DFO
HNK+DFO
D
NC
HNK
DFO
HNK+DFO
RKO
NC
HNK
DFO
HNK+DFO
SW480
E
RKO
SW480
NC
DFO
HNK+DFO
HNK
Count
DCFH-DA
F
RKO
SW480
NC
HNK
DFO
DFO+HNK
Transferrin
Ferropotin
GAPDH

Figure 2. HNK increased the levels of ROS and Fe^{2+} in CC cells. (A) We use DCFH-DA fluorescence probe to investigate the level of intracellular ROS in CC cells by a flow cytometer. The mean fluorescence intensity (MFI) was used to compare ROS levels in CC cells. (B) DFO has the effect of reversing ferroptosis process. We introduced it to rescue test, and the groups are as follows: the NC group, HNK group, DFO group, and HNK+DFO group. The survival rate of the cells in each group was measured by flow cytometry with Annexin V/PI staining kit. (C) Sytox green staining was used to assess cell death in different groups (original magnification: 200×). (D) The Mito-FerroGreen fluorescent dye kit was used to label Fe^{2+} ions, and the image of green fluorescence signal in the cytoplasm indicates the probe is specific, which are captured by confocal instrument. (E) The ROS level in CC cells were measured by flow cytometer. The ROS level in the DFO+HNK group was significantly decreased compared with that in the DFO group (P<0.05). (F) Western blot was used to determine the protein level of Transferrin and Ferroportin after incubation with HNK. Compared with NC group, the protein level of Transferrin increased significantly in the DFO+HNK group, and the protein level of Ferroportin also decreased sharply (P<0.05, (F)). All experiments were repeated in triplicate, and the data are shown as the mean ± SD values. Compared to NC group, *: P<0.05, **: P<0.01, ***: P<0.001, ****: P<0.0001. Compared to HNK group, #: P<0.05, ##: P<0.01.

Furthermore, treatment with DFO alone did not increase ROS levels (P>0.05, **Figure 2E**). However, the ROS level in the DFO+HNK group was significantly decreased compared with that in the DFO group (P<0.05, **Figure 2E**). After incubation with HNK, the protein level of Transferrin increased significantly, while that of Ferroportin decreased sharply (P<0.05, **Figure 2F**). Furthermore, after DFO treatment, the protein levels of both Transferrin and Ferroportin decreased significantly (P<0.05, **Figure 2F**).

Mitochondrial morphology was altered in cells treated with HNK

Specific ultrastructural changes also occurred in mitochondria after ferroptosis. As evidenced by electron microscopy, the size of intracellular mitochondria decreased, the membrane density increased, the mitochondrial ridge shrank or disappeared, and the bilayer membrane density increased. As shown in **Figure 3**, in SW480 and RKO cells, the mitochondrial membrane density increased and the mitochondrial ridge shrank or disappeared in the HNK-treated groups after 12 h of HNK treatment, as evidenced by transmission electron microscopy (20000× magnification). However, no significant abnormal changes occurred in mitochondria in the DFO groups. The mitochondrial volume was smaller in the HNK+DFO group than in the NC group, and the density of the mitochondrial membrane was higher in the HNK+DFO group than in the NC group. These results suggested that HNK treatment may induce ferroptosis-like changes in mitochondria.

HNK decreased the activity of GPX4 but did not affect system Xc-

Studies have repeatedly indicated that cell viability decreases in response to inactivation of GPX4, which results in the accumulation of lipid ROS on membranes. Therefore, we first investigated the influence of HNK on ROS. We found that HNK increased ROS level above, so we further investigated the influence of HNK on GPX4. As shown in **Figure 4A**, the GPX4 protein levels in the two CC cell lines decreased significantly in a concentration-dependent manner after exposure to HNK for 24 h (P<0.05, **Figure 4A**). To further verify the role of GPX4 in the HNK regulatory network, we constructed GPX4 overexpression plasmids and transfected CC cell lines with GPX4 overexpression plasmid or the vector plasmid. **Figure 4B** and **4E** showed a significant decrease in cell death in GPX4 overexpression cells when compared with the vector cells. In addition, the levels of both ROS and Fe^{2+} were significantly lower in the GPX4-OE overexpression group than in the vector group (**Figure 4C** and **4D**, P<0.05). These results suggested that GPX4 may be the key molecule that regulates HNK-induced ferroptosis in CC cells.

At the molecular level, the cystine/glutamic acid reverse exchange transporters (system Xc-) GSH and GPX4, which transport cystine, form a barrier to ferroptosis. Disrupting any of these links impacts the sensitivity of cells to ferroptosis. Therefore, we explored the effect of HNK on the level of upstream molecules in GPX4 regulatory networks. As shown in **Figure 4F**, HNK treatment did not change the levels of the upstream system Xc- factors glutamic acid or GSH level (P>0.05). Therefore, we concluded that HNK affects the ROS-induced cell death process mediated by GPX4-modulated Fe^{2+} iron level.

CC cell growth was inhibited by HNK in vivo

In vitro, the increase in ROS levels caused by GPX4 inactivation was identified as a key mech-

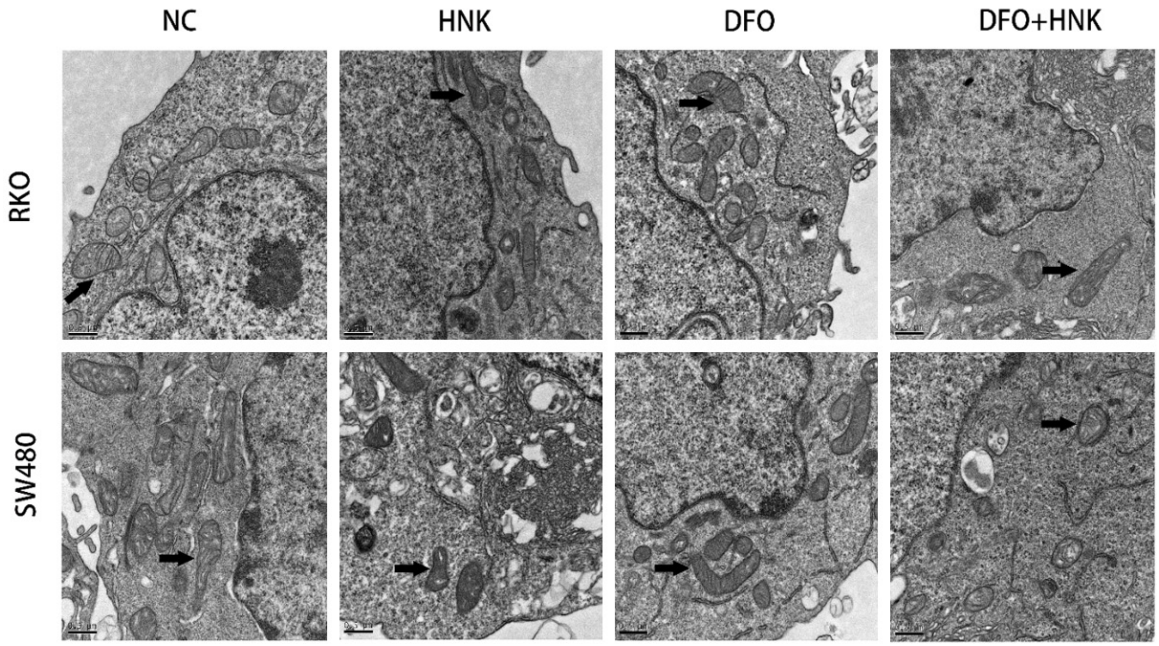

Figure 3. HNK induced changes in the mitochondrial morphology in cells. The transmission electron microscope was used to inspect mitochondrial morphology of cells. The mitochondrial morphologic changes of the cells in each group was pointed out by lack arrow in figure representively (20000× magnification). In the group of HNK-treated of SW480 and RKO, the density of the mitochondrial membrane increased and the mitochondrial ridge shrank or disappeared. There are no significant abnormal changes occurred in mitochondria in the DFO groups, as compared to NC group. The mitochondrial volume in the HNK+DFO group was smaller than that in the NC group, and the density of the mitochondrial membrane was higher than that in the NC group.

anism through which HNK kills CC cells. RKO cells stably overexpressing GPX4 (Lv-GPX4 cells) or normal control vector (Lv-NC cells) were generated, for establishing a xenograft model in nude mice via subcutaneous injection. **Figure 5A** shows that the tumor volumes and weights were significantly lower in the Lv-NC group than in the Lv-GPX4 group ($P< 0.05$). These results suggested that GPX4 is the key molecule through which HNK exerts its tumoricidal effects.

Discussion

Programmed and unprogrammed cell death mechanisms, including apoptosis, autophagy, and necrosis, are important processes of normal metabolism [23]. Approaches to induce tumor cell death efficiently and specifically have historically been the focus of numerous medical researchers [24].

In the current study, HNK, a low-toxicity plant extract from the Magnolia genus, was the main research object. HNK exerts significant anticancer effects in many kinds of human tumors via apoptosis and autophagy pathways [25, 26]. Consistent with these observations, we treated CC cells and found that HNK induced CC cell apoptosis. The chemical structure of HNK contains two phenol groups that may have antioxidant properties, namely, vitamin C and vitamin E. Reports indicate that HNK may function as a strong ROS scavenger in cell-free systems and melanoma cells. Interestingly, several reports indicate that HNK induces an increase in the ROS level in tumor cells [21, 27]. However, paradoxically, HNK may have both antioxidant and pro-oxidant activities. However, regarding these phenotypes, vitamins C and E consistently have similar characteristics, exhibiting both antioxidant and pro-oxidant effects [28-30]. Overall, these observations suggest that ROS production is a determining factor of HNK cytotoxicity. In this study, HNK significantly increased ROS accumulation in CC cells. However, the exact mechanism underlying the pro-oxidant activity of HNK is unclear in CC.

An increase in lipid peroxide levels is another characteristic of ferroptosis, and an increase in lipid ROS levels was detected in this study. We speculated that ferroptosis is also a molecular mechanism of HNK. To verify our hypothesis,

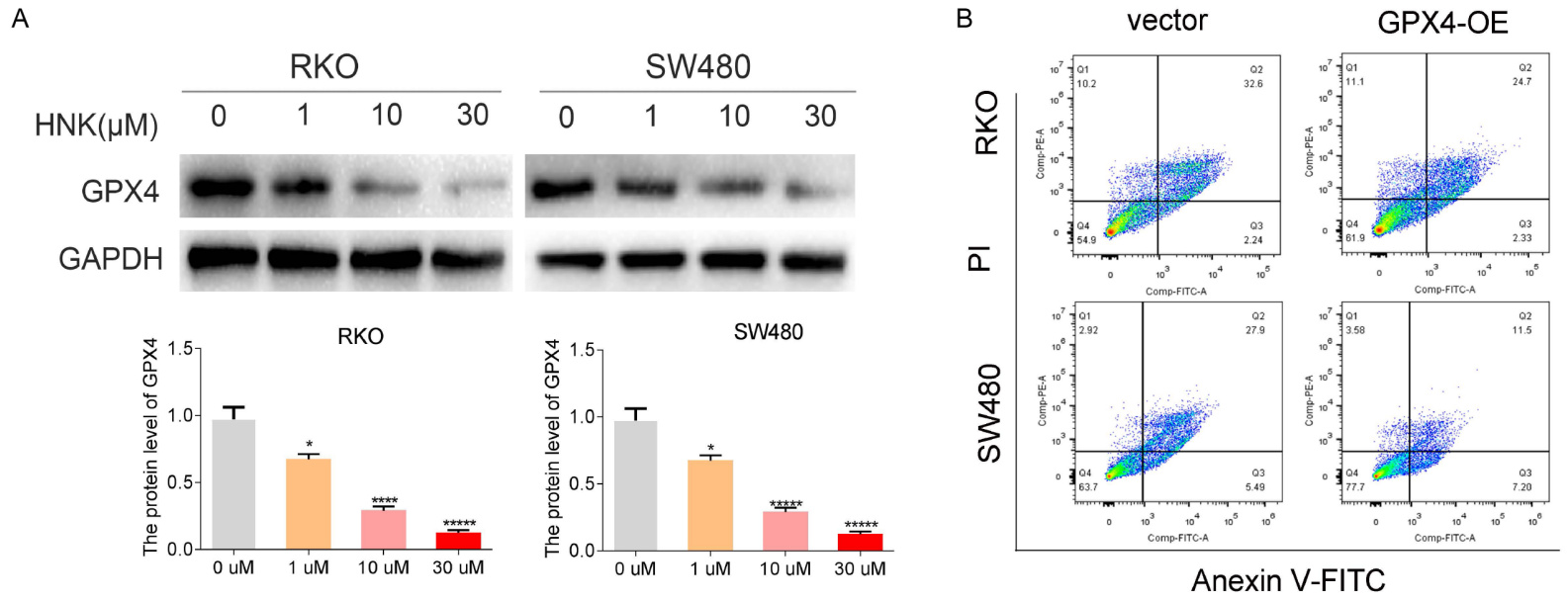
A
RKO
SW480
HNK(μM)
0
1
10
30
GPX4
GAPDH
The protein level of GPX4
0 uM
1 uM
10 uM
30 uM
B
vector
GPX4-OE
RKO
SW480
PI
Anexin V-FITC
Comp-PE-A
Comp-FITC-A

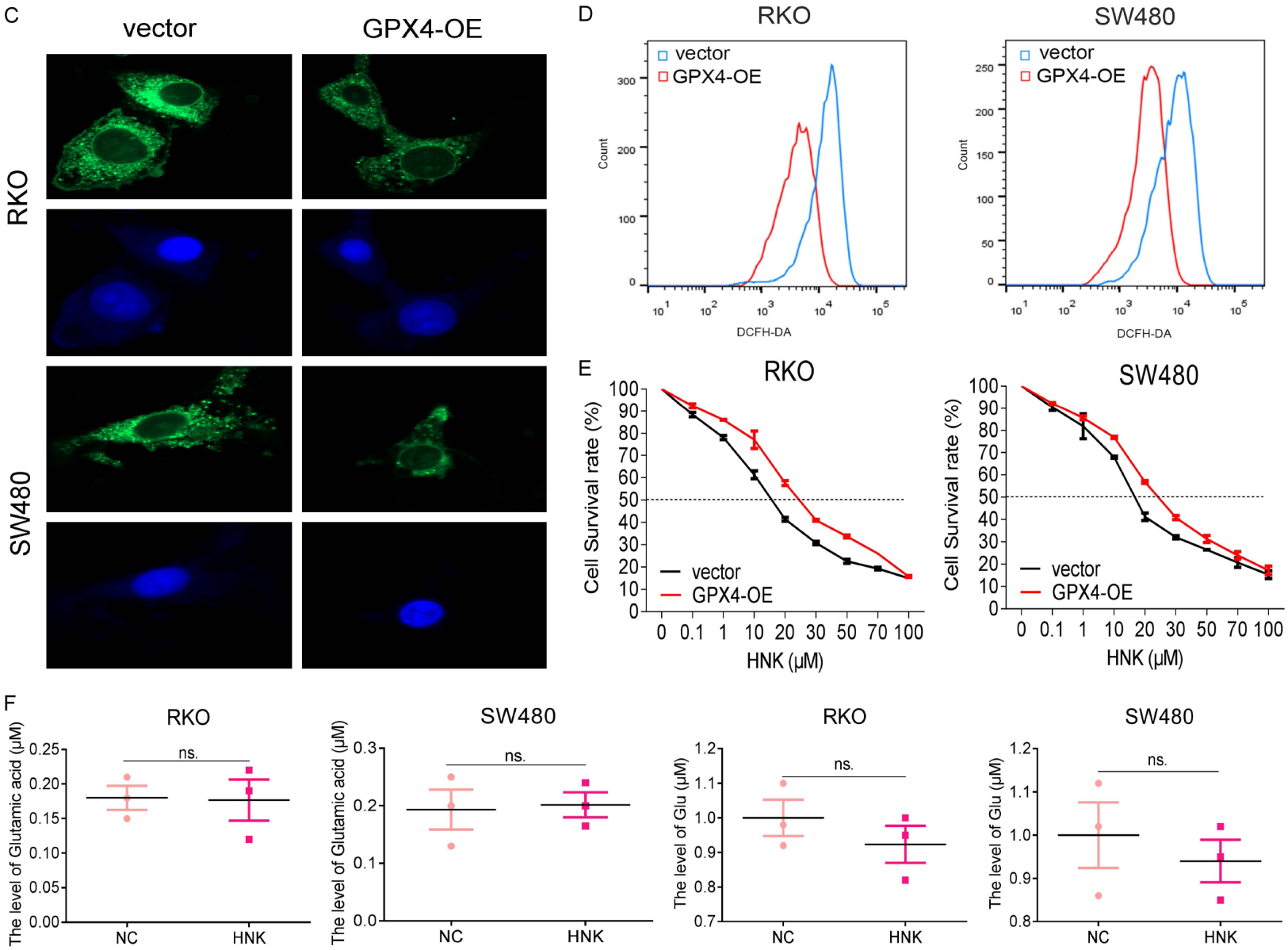

Figure 4. HNK decreased the activity of GPX4 but did not affect system Xc-. A. GPX4 protein expression was measured by Western blot analysis and was normalized to GAPDH protein expression. B. The cell death rates of CC cells with GPX4 overexpression were determined by flow cytometry with Annexin V/PI staining. C. The

Fe^{2+} level was determined with Mito-FerroGreen dye, which is captured by confocal instrument (original magnification: 400×). D. The level of ROS after overexpression of GPX4 in SW480 and RKO cell lines was investigated. E. To determine the effect of GPX4 overexpression on CC cells, a CCK8 assay was carried out to determine the IC_{50} values of HNK in CC cells after GPX4 overexpression. F. The levels of cystine and the intermediate product Glu in system Xc- upstream of GPX4 were measured. Compared to 0 μM group and vector group, *: $P<0.05$, **: $P<0.01$, ***: $P<0.001$, ****: $P<0.0001$.

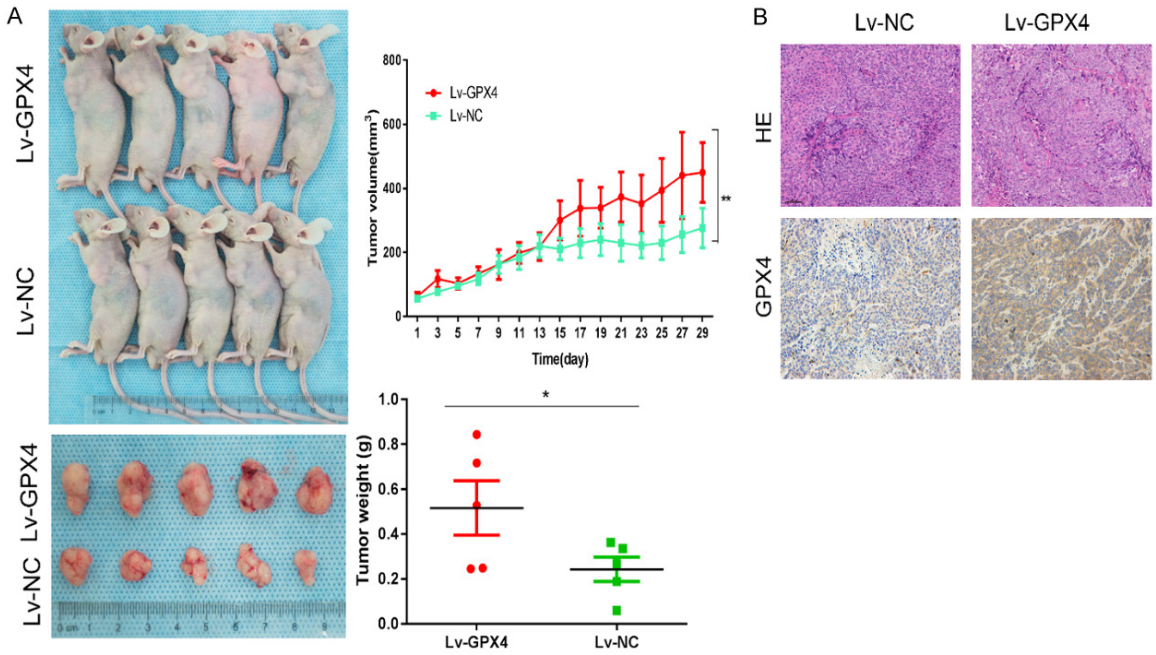

Figure 5. CC cell growth was inhibited by HNK in vivo. In vitro, the increase in ROS levels caused by GPX4 inactivation was identified as a key mechanism through which HNK kills CC cells. Thus, RKO cells stably overexpressing GPX4 were generated, and a xenograft model was established in nude mice via subcutaneous injection. A. The xenograft experiment showed that the tumor volumes and weights were significantly higher in the Lv-GPX4 group than in the Lv-NC group, as we recorded the subcutaneous tumor volume of each mouse every two days. B. Paraffin sections of subcutaneous tumors were carried and IHC was used to detect the level of GPX4 in xenograft tumors. The data shown that the protein level of GPX4 was significantly increased in the Lv-GPX4 group compared with the Lv-NC group (original magnification: 200×). The data are shown as the mean ± SD values. Compared to Lv-NC group, *: $P<0.05$, **: $P<0.01$.

we introduced the iron chelator DFO, a specific inhibitor of ferroptosis, and established multiple control groups to detect cell death rates [31]. Interestingly, DFO significantly reversed the important phenotypes of cell death induced by HNK and ferroptosis induced by ROS accumulation. Moreover, the cell death rate was significantly decreased with DFO treatment and, importantly, cellular ROS levels also decreased. These effects were confirmed by subsequent measurement of ROS and Fe^{2+} levels. Iron ions are the primary particles involved in the occurrence of ferroptosis. The stability of the cell iron pool is maintained under precise regulation by Transferrin and Ferroportin. After HNK treatment, the level of ferroportin decreased significantly. In contrast, the level of transferrin, which contributes to iron transport into cells, increased significantly.

Furthermore, specific ultrastructural changes occurred in mitochondria after ferroptosis. As evidenced by electron microscopy, the size of intracellular mitochondria decreased, the membrane density increased, the mitochondrial ridge shrank or disappeared, and the bilayer membrane density increased. As shown in **Figure 3**, after incubation with HNK for 12 h, intracellular mitochondria showed phenotypic changes typical of ferroptosis, including a decreased size, an increased membrane density, and a shrunken or absent mitochondrial ridge. We retrieved the recent documents on ferroptosis mechanisms, suggesting that the

mechanisms of ferroptosis can be classified GPX4 dependent and non GPX4 dependent regulatory pathways. (1). GPX4 dependent pathway. Direct or indirect regulation of GPX4 activity are considered the important mechanisms of ferroptosis [32]. New compounds DPI2 [33], FIN56 [34] and RSL3 [35] induce cell ferroptosis by direct or indirect inhibition of GPX4, to produce ROS. (2). non GPX4 dependent regulatory pathways. Recently, studies have indicated FSAP1 regulated ferroptosis signaling pathways, which independent of GPX4. Moreover, oxidative stress and autophagy are also involved in the regulation of ferroptosis [36-39]. However, GPX4 is the most classical and core regulatory mechanism of ferroptosis. By inhibiting GPX4 to induce ferroptosis, it is expected to be a therapeutic strategy to treat some cancers [40, 41].

Previous studies revealed that ferroptosis is induced by the inactivation of GPX4, which leads to the accumulation of reactive lipid ROS on membranes, and iron ions are essential players in ROS accumulation. Therefore, we first investigated the regulatory effect of HNK on GPX4. When CC cells were treated with HNK in a concentration gradient, the expression of GPX4 decreased. Then, we constructed GPX4-overexpressed plasmids and found that overexpression of GPX4 significantly decreased the antitumor effect of HNK in vitro, suggesting that GPX4 may be a vital regulator of HNK-induced CC cell death. Furthermore, by investigating the classical ferroptosis inducers reported to date, we found that ferroptosis inducers are divided into two main molecular types. By regulating cystine/glutamic acid antiporter (system Xc-), affects the formation of Glu, the substrate of GPX4, and like erastin, indirectly affects the activity of GPX4. Inhibitors of the other molecular type, for example, RSL3, directly target GPX4 to promote the formation of lipid peroxides. According to one study [42], overexpression of GPX4 suppresses RSL3-induced ferroptosis. However, knockdown of GPX4 enhances it, suggesting that inhibition of GPX4 activity contributes to ferroptosis. In this study, HNK-induced CC cell death decreased the GPX4 protein level in a concentration way. In most recent studies, at the molecular level, system Xc-, which transports cystine, as well as GSH and GPX4, form a barrier to ferroptosis. Disrupting any of these links increases the sensitivity of cells to ferroptosis. Therefore, as an important regulatory pathway of GPX4 dependence, the Xc- system was investigated furtherly which indirectly deactivates GPX4 by depleting substrate GSH thereby. We explored the expression of cystine and the intermediate product GSH system Xc- upstream of GPX4 and found that HNK did not affect the level of molecules related to system Xc-. These datas suggested that GPX4 to be a key molecule HNK mediates ferroptosis in CC cells *in vitro*. Furthermore, we constructed a stable cell line overexpressing GPX4 and used a subcutaneous xenograft model for *in vivo* experiment. The tumor volumes were significantly lower in the vector group than in the GPX4 overexpression group (**Figure 5A**).

In conclusion, Our datas showed that HNK can induce ferroptosis in CC cells and play a role in GPX4 dependent pathway, which suggest a new clue and theoretical support for the antitumor activity of CC cancer.

Conclusions

HNK induces ferroptosis in CC cells by reducing the activity of GPX4. As a potential therapeutic drug, HNK showed good anticancer effects through a variety of signal transduction mechanisms and multiple pathways.

Acknowledgements

This study was supported by grants from National Key R&D Program of China (No. 2018YFC1313300), National Natural Science Foundation of China (No.: 81070362, 81172470, 81372629, 81772627, 81874073, 81974384 & 81902500), key projects from the Nature Science Foundation of Hunan Province (No. 2015JC3021 & 2016JC2037), two projects from CSCO Cancer Research Foundation (No. Y-HR2019-0182 & Y-2019Genecast-043). All animal experiments and procedures were directed and approved by the Experimental Animal Ethics Committee of Central South University.

Disclosure of conflict of interest

None.

Abbreviations

HNK, Honokiol; ROS, Reactive Oxygen Species; CC, Colon cancer; GPX4, Glutathione Peroxidase 4; DFO, Deferoxamine; FPN1, Ferroportin; TFR, Transferrin.

Address correspondence to: Dr. Gongping Deng, Department of Emergency, Hainan General Hospital, Hainan Affiliated Hospital of Hainan Medical University, 19 Xiuhua Road, Haikou 570311, Hainan, China. Tel: +86-18808987878; E-mail: denggongping@hainmc.edu.cn; Dr. Shan Zeng, Department of Oncology, Xiangya Hospital, Central South University, Changsha 410008, Hunan, China. Tel: +86-731-89753034; E-mail: zengshan2000@csu.edu.cn

References

[1] Zhu Y, Wei W, Ye T, Liu Z, Liu L, Luo Y, Zhang L, Gao C, Wang N and Yu L. Small molecule TH-39 potentially targets Hec1/Nek2 interaction and exhibits antitumor efficacy in K562 cells via G0/G1 cell cycle arrest and apoptosis induction. Cell Physiol Biochem 2016; 40: 297-308.

[2] Deng G, Zeng S, Ma J, Zhang Y, Qu Y, Han Y, Yin L, Cai C, Guo C and Shen H. The anti-tumor activities of Neferine on cell invasion and oxaliplatin sensitivity regulated by EMT via Snail signaling in hepatocellular carcinoma. Sci Rep 2017; 7: 41616.

[3] Deng G, Zeng S, Qu Y, Luo Q, Guo C, Yin L, Han Y, Li Y, Cai C, Fu Y and Shen H. BMP4 promotes hepatocellular carcinoma proliferation by autophagy activation through JNK1-mediated Bcl-2 phosphorylation. J Exp Clin Cancer Res 2018; 37: 156.

[4] Pistritto G, Trisciuoglio D, Ceci C, Garufi A and D'Orazi G. Apoptosis as anticancer mechanism: function and dysfunction of its modulators and targeted therapeutic strategies. Aging (Albany NY) 2016; 8: 603-619.

[5] Xavier CP, Pesic M and Vasconcelos MH. Understanding cancer drug resistance by developing and studying resistant cell line models. Curr Cancer Drug Targets 2016; 16: 226-237.

[6] Doll S and Conrad M. Iron and ferroptosis: a still ill-defined liaison. IUBMB Life 2017; 69: 423-434.

[7] Dixon SJ, Lemberg KM, Lamprecht MR, Skouta R, Zaitsev EM, Gleason CE, Patel DN, Bauer AJ, Cantley AM, Yang WS, Morrison BR and Stockwell BR. Ferroptosis: an iron-dependent form of nonapoptotic cell death. Cell 2012; 149: 1060-1072.

[8] Xie Y, Hou W, Song X, Yu Y, Huang J, Sun X, Kang R and Tang D. Ferroptosis: process and function. Cell Death Differ 2016; 23: 369-379.

[9] Latunde-Dada GO. Ferroptosis: role of lipid peroxidation, iron and ferritinophagy. Biochim Biophys Acta Gen Subj 2017; 1861: 1893-1900.

[10] Fanzani A and Poli M. Iron, oxidative damage and ferroptosis in rhabdomyosarcoma. Int J Mol Sci 2017; 18: 1718.

[11] Cao JY and Dixon SJ. Mechanisms of ferroptosis. Cell Mol Life Sci 2016; 73: 2195-2209.

[12] Gao M, Monian P, Quadri N, Ramasamy R and Jiang X. Glutaminolysis and transferrin regulate ferroptosis. Mol Cell 2015; 59: 298-308.

[13] Dixon SJ and Stockwell BR. The role of iron and reactive oxygen species in cell death. Nat Chem Biol 2014; 10: 9-17.

[14] Huo H, Zhou Z, Qin J, Liu W, Wang B and Gu Y. Erastin disrupts mitochondrial permeability transition pore (mPTP) and induces apoptotic death of colorectal cancer cells. PLoS One 2016; 11: e0154605.

[15] Dachert J, Schoeneberger H, Rohde K and Fulda S. RSL3 and Erastin differentially regulate redox signaling to promote Smac mimetic-induced cell death. Oncotarget 2016; 7: 63779-63792.

[16] Lorincz T, Jemnitz K, Kardon T, Mandl J and Szarka A. Ferroptosis is involved in acetaminophen induced cell death. Pathol Oncol Res 2015; 21: 1115-1121.

[17] Sehm T, Fan Z, Ghoochani A, Rauh M, Engelhorn T, Minakaki G, Dorfler A, Klucken J, Buchfelder M, Eyupoglu IY and Savaskan N. Sulfasalazine impacts on ferroptotic cell death and alleviates the tumor microenvironment and glioma-induced brain edema. Oncotarget 2016; 7: 36021-36033.

[18] Lin R, Zhang Z, Chen L, Zhou Y, Zou P, Feng C, Wang L and Liang G. Dihydroartemisinin (DHA) induces ferroptosis and causes cell cycle arrest in head and neck carcinoma cells. Cancer Lett 2016; 381: 165-175.

[19] Prasad R and Katiyar SK. Honokiol, an active compound of magnolia plant, inhibits growth, and progression of cancers of different organs. Adv Exp Med Biol 2016; 928: 245-265.

[20] Pan J, Lee Y, Wang Y and You M. Honokiol targets mitochondria to halt cancer progression and metastasis. Mol Nutr Food Res 2016; 60: 1383-1395.

[21] Lin CJ, Chen TL, Tseng YY, Wu GJ, Hsieh MH, Lin YW and Chen RM. Honokiol induces autophagic cell death in malignant glioma through reactive oxygen species-mediated regulation of the p53/PI3K/Akt/mTOR signaling pathway. Toxicol Appl Pharmacol 2016; 304: 59-69.

[22] Lu CH, Chen SH, Chang YS, Liu YW, Wu JY, Lim YP, Yu HI and Lee YR. Honokiol, a potential therapeutic agent, induces cell cycle arrest and program cell death in vitro and in vivo in human thyroid cancer cells. Pharmacol Res 2017; 115: 288-298.

[23] De Felici M and Piacentini M. Programmed cell death in development and tumors. Int J Dev Biol 2015; 59: 1-3.

[24] Xie Y, Song X, Sun X, Huang J, Zhong M, Lotze MT, Zeh HJR, Kang R and Tang D. Identification

of baicalein as a ferroptosis inhibitor by natural product library screening. Biochem Biophys Res Commun 2016; 473: 775-780.
[25] Balan M, Chakraborty S, Flynn E, Zurakowski D and Pal S. Honokiol inhibits c-Met-HO-1 tumor-promoting pathway and its cross-talk with calcineurin inhibitor-mediated renal cancer growth. Sci Rep 2017; 7: 5900.
[26] Godugu C, Doddapaneni R and Singh M. Honokiol nanomicellar formulation produced increased oral bioavailability and anticancer effects in triple negative breast cancer (TNBC). Colloids Surf B Biointerfaces 2017; 153: 208-219.
[27] Huang K, Chen Y, Zhang R, Wu Y, Ma Y, Fang X and Shen S. Honokiol induces apoptosis and autophagy via the ROS/ERK1/2 signaling pathway in human osteosarcoma cells in vitro and in vivo. Cell Death Dis 2018; 9: 157.
[28] Hail N Jr and Lotan R. Cancer chemoprevention and mitochondria: targeting apoptosis in transformed cells via the disruption of mitochondrial bioenergetics/redox state. Mol Nutr Food Res 2009; 53: 49-67.
[29] Hahm ER and Singh SV. Honokiol causes G0-G1 phase cell cycle arrest in human prostate cancer cells in association with suppression of retinoblastoma protein level/phosphorylation and inhibition of E2F1 transcriptional activity. Mol Cancer Ther 2007; 6: 2686-2695.
[30] Pan J, Zhang Q, Liu Q, Komas SM, Kalyanaraman B, Lubet RA, Wang Y and You M. Honokiol inhibits lung tumorigenesis through inhibition of mitochondrial function. Cancer Prev Res (Phila) 2014; 7: 1149-1159.
[31] Jelinek A, Heyder L, Daude M, Plessner M, Krippner S, Grosse R, Diederich WE and Culmsee C. Mitochondrial rescue prevents glutathione peroxidase-dependent ferroptosis. Free Radic Biol Med 2018; 117: 45-57.
[32] Friedmann Angeli JP, Schneider M, Proneth B, Tyurina YY, Tyurin VA, Hammond VJ, Herbach N, Aichler M, Walch A, Eggenhofer E, Basavarajappa D, Rådmark O, Kobayashi S, Seibt T, Beck H, Neff F, Esposito I, Wanke R, Förster H, Yefremova O, Heinrichmeyer M, Bornkamm GW, Geissler EK, Thomas SB, Stockwell BR, O'Donnell VB, Kagan VE, Schick JA and Conrad M. Inactivation of the ferroptosis regulator Gpx4 triggers acute renal failure in mice. Nat Cell Biol 2014; 16: 1180-91.
[33] Yang WS, SriRamaratnam R, Welsch ME, Shimada K, Skouta R, Viswanathan VS, Cheah JH, Clemons PA, Shamji AF, Clish CB, Brown LM, Girotti AW, Cornish VW, Schreiber SL and Stockwell BR. Regulation of ferroptotic cancer cell death by GPX4. Cell 2014; 156: 317-331.
[34] Shimada K, Skouta R, Kaplan A, Yang WS, Hayano M, Dixon SJ, Brown LM, Valenzuela CA, Wolpaw AJ and Stockwell BR. Global survey of cell death mechanisms reveals metabolic regulation of ferroptosis. Nat Chem Biol 2016; 12: 497-503.
[35] Ye Z, Hu Q, Zhuo Q, Zhu Y, Fan G, Liu M, Sun Q, Zhang Z, Liu W, Xu W, Ji S, Yu X, Xu X and Qin Y. Abrogation of ARF6 promotes RSL3-induced ferroptosis and mitigates gemcitabine resistance in pancreatic cancer cells. Am J Cancer Res 2020; 10: 1182-1193.
[36] Doll S, Freitas FP, Shah R, Aldrovandi M, da Silva MC, Ingold I, Goya Grocin A, Xavier da Silva TN, Panzilius E, Scheel CH, Mourão A, Buday K, Sato M, Wanninger J, Vignane T, Mohana V, Rehberg M, Flatley A, Schepers A, Kurz A, White D, Sauer M, Sattler M, Tate EW, Schmitz W, Schulze A, O'Donnell V, Proneth B, Popowicz GM, Pratt DA, Angeli JPF and Conrad M. FSP1 is a glutathione-independent ferroptosis suppressor. Nature 2019; 575: 693-698.
[37] Bersuker K, Hendricks JM, Li Z, Magtanong L, Ford B, Tang PH, Roberts MA, Tong B, Maimone TJ, Zoncu R, Bassik MC, Nomura DK, Dixon SJ and Olzmann JA. The CoQ oxidoreductase FSP1 acts parallel to GPX4 to inhibit ferroptosis. Nature 2019; 575: 688-692.
[38] Guo S, Jiang S, Epperla N, Ma Y, Maadooliat M, Ye Z, Olson B, Wang M, Kitchner T, Joyce J, An P, Wang F, Strenn R, Mazza JJ, Meece JK, Wu W, Jin L, Smith JA, Wang J and Schrodi SJ. A gene-based recessive diplotype exome scan discovers FGF6, a novel hepcidin-regulating iron-metabolism gene. Blood 2019; 133: 1888-1898.
[39] Liu J, Kuang F, Kroemer G, Klionsky DJ, Kang R and Tang D. Autophagy-dependent ferroptosis: machinery and regulation. Cell Chem Biol 2020; 27: 420-435.
[40] Hassannia B, Vandenabeele P and Vanden Berghe T. Targeting ferroptosis to iron out cancer. Cancer Cell 2019; 35: 830-849.
[41] Mou Y, Wang J, Wu J, He D, Zhang C, Duan C and Li B. Ferroptosis, a new form of cell death: opportunities and challenges in cancer. J Hematol Oncol 2019; 12: 34.
[42] Yang WS, SriRamaratnam R, Welsch ME, Shimada K, Skouta R, Viswanathan VS, Cheah JH, Clemons PA, Shamji AF, Clish CB, Brown LM, Girotti AW, Cornish VW, Schreiber SL and Stockwell BR. Regulation of ferroptotic cancer cell death by GPX4. Cell 2014; 156: 317-331.